Autoionization and photoionization of O(^1D)

R. Flesch, M. C. Schürmann, J. Plenge, H. Meiss, M. Hunnekuhl, and E. Rühl
Fachbereich Physik, Universität Osnabrück, Barbarastrasse 7, D-49069 Osnabrück, Germany
(Received 22 February 2000; revised manuscript received 19 June 2000; published 19 October 2000)

Single-photon ionization of atomic singlet oxygen [O(^1D)] is investigated between 12 and 18 eV. O(^1D) is efficiently prepared by laser photolysis of ozone in the Hartley band regime ($\lambda = 270$ nm). It is subsequently ionized by using monochromatic radiation, which is generated in a laser-produced plasma. Time-of-flight mass spectra are recorded and the photoion yield of O^+ is measured. Direct photoionization of O(^1D) is not observed between the onset of the first ($^4S^o$) and the second ($^2D^o$) ionization threshold. Intense resonant features occur below the $^2D^o$ threshold. These are assigned to *LS*-forbidden autoionization of Rydberg singlet states by the $^4S^o$ continuum. The relative intensities of autoionization resonances are compared to the corresponding optical oscillator strengths. The results are discussed in terms of the autoionization efficiency of Rydberg states.

PACS number(s): 32.80.Dz, 32.80.Fb

I. INTRODUCTION

The first excited state of atomic oxygen O(^1D) is of considerable interest in atmospheric research, since it is efficiently deactivated by reactive or nonreactive collisions with atmospheric constituents [1]. The major source of atmospheric O(^1D) is ozone, which is photolyzed by ultraviolet radiation [2]. In addition, O(^1D) is also known to play an important role in plasma physics and astrophysics [3].

The electronic configuration of atomic oxygen $1s^2 2s^2 2p^4$ is known to generate the ^3P ground state as well as the lowest excited states ^1D and ^1S [4–6]. The energy of O(^1D) is increased relative to that of O(^3P) by 1.967 36 eV [7].

Photoexcitation and photoionization of O(^1D) have been the subject of various experimental and theoretical studies in the past [8–18]. The cation O^+ ($1s^2 2s^2 2p^3$) has a $^4S^o$ ground state; its first excited states are [6] $^2D^o$ [$E(^2D_{5/2}) = 16.9421$ eV, $E(^2D_{3/2}) = 16.9446$ eV] and $^2P^o$ ($E = 18.6355$ eV), where the energy values are given relative to O(^3P) [8]. Single photon ionization allows transitions from the ^3P ground state into these O^+ levels. Earlier work predicted that direct photoionization of O(^1D) into the $^4S^o$ state is spin-forbidden [19], so that the onset of direct photoionization is expected to occur at the $^2D^o$ threshold. This is in accordance with the dipole selection rule $\Delta S = 0$, since the running electron generates only triplet and quintet states.

The optical spectrum of O(^1D) has been investigated by Huffman and co-workers in the 13–17-eV regime [9], where several Rydberg series of singlet states were observed that converge towards the $^2D^o$ and $^2P^o$ ionization limits of O(^1D). A variety of states can be generated as a result of the excited $2p^3 n\ell$ configuration [6], where predominantly singlet states ($^1P^o$, $^1D^o$, and $^1F^o$) occur in optical spectroscopy [9]. Earlier work by Huffman *et al.* indicated that low-lying Rydberg states were observed in emission, whereas the higher members are found in absorption [9,20]. This has been rationalized in terms of nonautoionizing low-lying Rydberg states, which were primarily observed in emission. Photoionization experiments on ground state O(^3P) indicate that autoionization processes may compete with radiative decay processes [21,22], where the branching ratio between autoionization and fluorescence has been measured for several $^3P^o$ Rydberg states [23]. Autoionization of singlet Rydberg states converging to the $^2D^o$ and $^2P^o$ thresholds via the $^4S^o$ continuum is forbidden in LS coupling [4]. However, autoionization may occur as a result of second-order processes, for example spin-other-orbit or spin-spin interaction [5]. Selection rules of such processes have been applied to autoionizing states of atomic oxygen [21–23].

The competition between autoionization and direct photoionization of O(^1D) has been investigated earlier by multiphoton laser techniques [10,11]. Two-photon transitions lead to ($^2D^o$)$3p\,^1F_3$ and ($^2D^o$)$3p\,^1P_1$ levels which autoionize into the $^4S^o$ continuum. In addition, the $^1F_3$ level undergoes autoionization as well as resonant transitions into higher excited Rydberg states, since the autoionization frequency of this state is low [11]. These levels are not accessible in one-photon transitions of O(^1D), so that they were not observed in previous work [9]. Recent experiments have been carried out by Richter and Hynes, who used ozone as a precursor of O(^1D) [12]. Photolysis of ozone in the Hartley band regime and subsequent three-photon absorption led in their experiments to the formation of various ($^2D^o$)$3d$ states ($^1F_3$, $^1D_2$, $^1P_1$, and $^1G_4$). In addition, the formation of the $^3G_4$ state was observed. The occurrence of states, such as $^1G_4$ and $^3G_4$, are a clear indication of multiphoton processes.

Extensive theoretical work on transitions within the O(I) system has been compiled by Wiese *et al.* [18]. High-level calculations have been carried out, where transition probabilities were calculated for a variety of singlet transitions [18]. Calculations on the photoionization cross section of O(^1D) have also been performed [13–17], where more recent work includes autoionizing Rydberg states above the second ($^2D^o$) ionization limit [16,17].

Single-photon ionization of O(^1D) has not been reported in the literature to the best of our knowledge. We present in this paper the photoion yield of O^+ from O(^1D) under experimental conditions where exclusively single-photon ionization occurs. Laser-produced plasma (LPP) radiation is a suitable high-intensity extreme ultraviolet (XUV) light

source [24–27]. We have recently shown that LPP radiation can be used as a broadband light source to investigate photoion yields of primary photofragments [28]. This light source is considerably more easily tunable over wide energy regimes than XUV laser sources that we have used in earlier work [29,30].

II. EXPERIMENT

A detailed description of the experimental setup has been published recently [28]. Briefly, it consists of the following major components: (i) a tunable, excimer-pumped pulsed dye-laser (Lambda Physik: Compex 201 and Scanmate) equipped with a frequency doubling unit [potassium dihydrogen phosphate (KDP) crystal]; (ii) a pulsed, tunable XUV light source that delivers monochromatic LPP radiation in the energy regime 8 eV$\leqslant E \leqslant$25 eV [the LPP radiation consists essentially of a broad background continuum [28]. It is dispersed by a 1 m vacuum monochromator (McPherson Nova 225) which is equipped with a 1200 $\diagup$/mm holographically ruled grating]; and (iii) a time-of-flight mass spectrometer (TOF) for cation separation and detection.

Neat ozone (O_3) is used for $O(^1D)$ production. The sample is prepared by flowing molecular oxygen through a laboratory ozonizer (Sander). The resulting O_3/O_2 mixture is trapped over liquid nitrogen. Subsequently, the mixture is purified by pumping at increased temperature, where liquid oxygen is used as a coolant. The residue consists almost exclusively of neat ozone. Photoionization mass spectrometry is used to control the purity of the sample, indicating that there are only minor impurities of molecular oxygen. This sample is subsequently used for $O(^1D)$ production by photolyzing O_3 at $\lambda = 270$ nm from a dye laser with a typical output power of $\approx$1 mJ/pulse at a repetition rate of 10 Hz. The nascent photofragments of ozone are primarily $O(^1D)$ and $O_2(a\,^1\Delta_g)$ [2,12]. They are subsequently photoionized by monochromatic time-correlated LPP radiation, yielding cations that are detected by the TOF mass spectrometer. The time delay between the photolysis laser and the XUV pulse is of the order of 100 ns. Photoion yields of O^+ are obtained by selecting this mass in the TOF mass spectrum while scanning the XUV photon energy. The slit width of the vacuum monochromator is set to 500 μm, corresponding to a wavelength resolution of 0.6 nm. The spectra are normalized with respect to the XUV photon flux and corrected for background contributions which result from ionic fragmentation of ozone into the O^+ channel. The wavelength scale of the vacuum monochromator is calibrated by using the well-known emission lines of rare gases, such as argon and krypton [31].

III. RESULTS AND DISCUSSION

Figure 1 shows a series of mass spectra of ozone that are obtained from different excitation conditions. The bottom spectrum [Fig. 1(a)] shows the mass spectrum of ozone, which is recorded at 13.45 eV photon energy. The most intense mass signals are due to O_3^+ ($m/z=48$, $t=4.496$ μs) and O_2^+ ($m/z=32$, $t=3.676$ μs). The adiabatic ionization

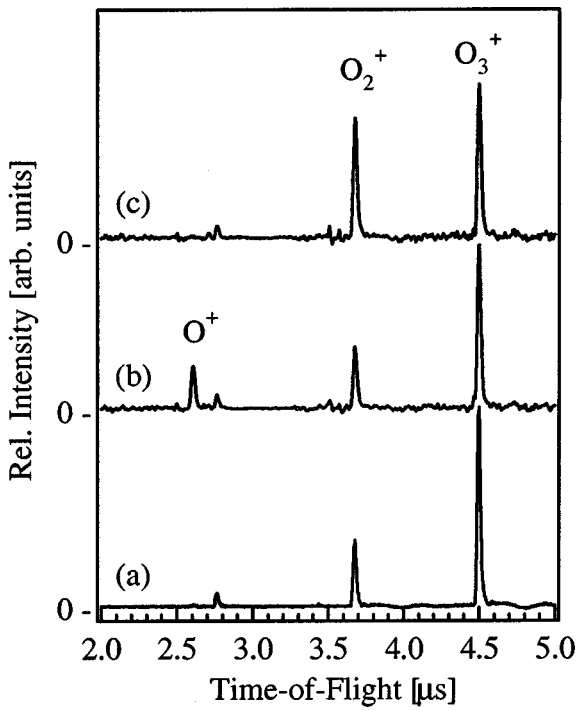

FIG. 1. Series of photoionization mass spectra of ozone: (a) photoionization at $E=13.45$ eV; (b) primary photolysis at $\lambda=270$ nm and subsequent photoionization at $E=13.45$ eV; (c) as (b), photoionization at $E=13.75$ eV.

energy of ozone is $I_E(O_3)=12.519\pm0.004$ eV, yielding the stable parent cation O_3^+ [32]. The O_2^+ mass signal is predominantly the result of ionic fragmentation of O_3^+. The onset energy of this process is 13.08 eV, yielding $O_2^+(X(^2\Pi))+O(^3P)$ [32]. The weak signal occurring at $t=2.602$ μs is due to O^+. This signal is not expected to be present at 13.45 eV photon energy since the onset of O^+ formation is observed at 15.21 ± 0.10 eV [32]. However, earlier work indicated that dispersed LPP-generated XUV radiation contains second-order light at $E\approx13$ eV [28]. Therefore, the weak O^+ signal is attributed to ionic fragmentation of ozone that comes from weak contributions of second-order radiation ($E=26.9$ eV), which are estimated to be of the order of 5%.

Figure 1(b) shows the photoionization mass spectrum at $E=13.45$ eV that is obtained after primary photolysis of ozone at $\lambda=270$ nm. The relative intensities of the mass signals discussed above change significantly as a result of the primary photolysis. The O_3^+ signal decreases by about 20%, whereas a strong increase of the O^+ signal is observed. Figure 1(c) shows a mass spectrum that is also obtained from the primary photolysis at $\lambda=270$ nm, but the XUV photon energy is slightly increased by 300 meV relative to the conditions used for recording the mass spectrum shown in Fig. 1(b) ($E=13.75$ eV). The O^+ signal has almost disappeared reaching a signal strength similar to that shown in Fig. 1(a). In contrast, the O_2^+ intensity has increased by a factor of $\approx$2.5. This result indicates that both the O_2^+ and the O^+ signals depend strongly upon the XUV photon energy.

The mass signals are attributed to the following photolysis

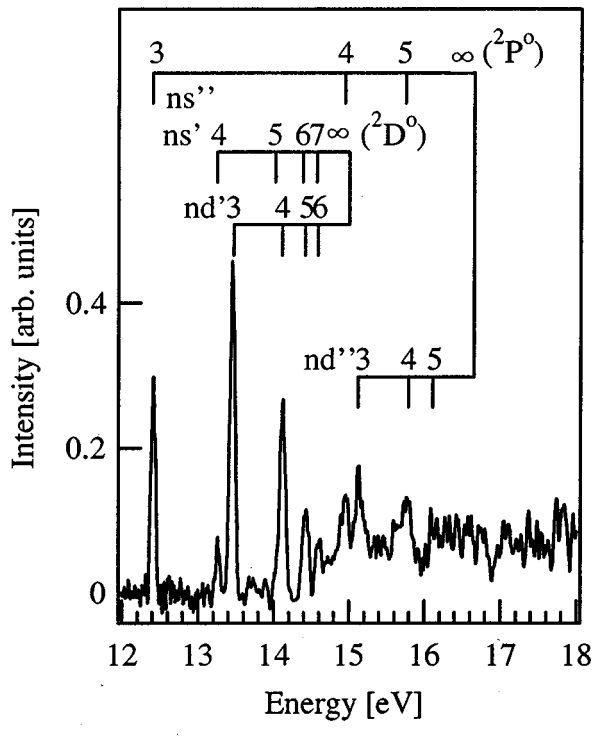

FIG. 2. Photoion yield of O^+ obtained from photoexcitation of O^1D). Contributions to the O^+ yield resulting from ionic fragmentation of ozone are subtracted. See text for further details.

and consecutive photoionization processes, where subsequent fragmentation of the molecular cations is not considered:

$$O_3(^1A_1) \xrightarrow{\lambda=270\ \mathrm{nm}} O(^1D) + O_2(a\,^1\Delta_g), \tag{1}$$

$$O_3(^1A_1) \xrightarrow{E=13.45\ \mathrm{eV}} O_3{}^+ + e^-, \tag{2a}$$

$$O_2(a\,^1\Delta_g) \xrightarrow{E=13.45\ \mathrm{eV}} O_2{}^+ + e^-, \tag{2b}$$

$$O(^1D) \xrightarrow{E=13.45\ \mathrm{eV}} O^+ + e^-. \tag{2c}$$

Step (1) represents the dominant photolysis channel of ozone in the Hartley band regime. Its quantum yield is known to be ≈ 0.9 [33]. The other minor channel leads to the ground state products $[O(^3P) + O_2(^3\Sigma_g^-)]$, where the molecular fragment is formed highly vibrationally excited [34]. We find no significant evidence for this minor channel so that it is not considered in this work. Step (2a) is due to photoionization of unphotolyzed ozone, whereas steps (2b) and (2c) describe photoionization of its photolysis products. We focus in the following exclusively on photoionization of $O(^1D)$ [cf. Eq. (2c)].

The modulation of the O^+ intensity in the mass spectra shown in Fig. 1 indicates that the formation of O^+ is the result of autoionization, similar to previous results from multiphoton ionization [10–12]. The tunability of the XUV light source allows us to measure the O^+ intensity in a wide energy regime, as shown in Fig. 2.

Photolytical formation and subsequent ionization of $O(^1D)$ are considered to be the dominant sources of the O^+ yield. However, there are additional sources that contribute to the O^+ channel under the present experimental conditions, such as ionic fragmentation of ozone [32] and the companion photoproduct $O_2(a\,^1\Delta_g)$. The contribution of the former process is determined by measuring the O^+ yield under identical experimental conditions, while keeping the photolysis laser turned off. The spectrum shown in Fig. 2 corresponds to the difference between the raw O^+ yield obtained from pump-probe conditions and the O^+ yield that is formed from neat O_3. This correction is $<5\%$ below 15.5 eV; it increases to $\approx 20\%$ at 18 eV. In addition, fragmentation of $O_2{}^+$ that is formed via photoionization of $O_2(a\,^1\Delta_g)$ is also expected to yield O^+ [cf. Eq. (2b)]. Its possible contribution to the O^+ yield is assumed to have little relevance below 18 eV, since the threshold of O^+ formation from photoionization of vibrationless $O_2(a\,^1\Delta_g)$ is calculated to be 17.66 eV, according to standard data tables [35,36]. Therefore, we have not considered this decay channel for Fig. 2.

Intense resonances are observed in Fig. 2. The intensity of the O^+ signal between these resonances drops almost to zero at photon energies $\leqslant 14$ eV. This indicates that there is no detectable background continuum on which the resonant features are superimposed. This is anticipated for photoionization of $O(^1D)$, because the direct optical transition of the excited atom into the $(^4S^o + \epsilon\ell)$ ionization continua is spin-forbidden. Similar results have been obtained earlier where multiphoton excitation has been used in order to ionize $O(^1D)$ [10–12]. The energy positions of the resonances are in agreement with previous optical data [9]. Therefore, all features that are found in the O^+ yield are assigned to transitions from $O(^1D)$ into excited singlet Rydberg states (see Fig. 2). A practical short-hand notation is used in the following in order to distinguish differently excited Rydberg states. These consist of a O^+ core and a Rydberg electron: $^2D^o$ core states are denoted by a single prime (e.g., $3d'$ denotes a Rydberg state with $^2D^o$ $3d$ configuration), $^2P^o$ corresponds to a double prime, and $^4S^o$ cores are indicated by no prime.

Huffman *et al.* have found four singlet series (ns': $^1D_2^o$; nd': $^1F_3^o$, $^1D_2^o$, $^1P_1^o$) that converge towards the $^2D^o$ threshold [$E_{5/2}=14.975$ eV relative to $O(^1D)$] and two further series (ns'': $^1P_1^o$; nd'': $^1D_2^o$) that converge to the $^2P^o$ ionization limit [$E=16.668$ eV relative to $O(^1D)$] [9]. The moderate wavelength resolution of the XUV radiation does not allow us to resolve the three close-lying nd' series so that they appear in Fig. 2 as a single blended line. Similarly, higher members of the nd' series are also blended with the ns' series.

The present results suggest that autoionization is an important relaxation route for singlet Rydberg states that are generated by single photon excitation from $O(^1D)$. Autoionization is observed below as well as above the second ($^2D^o$) ionization limit [8,9]. This process is in agreement with expectations from LS-selection rules in the $^2D^o$ continuum. In contrast, below this continuum, general selection rules for autoionization need to be considered [4,21–23]. This implies that the autoionizing term must have the same parity and

total angular momentum J as the energetically accessible ionization continuum. Moreover, in the case of LS coupling, the values of L and S of the autoionizing Rydberg state and the continuum must be the same. The continua between the first ($^4S^o$) and the second ($^2D^o$) ionization threshold of atomic oxygen are $^3S^o_1$, $^5S^o_2$, $^3D^o_{3,2,1}$, and $^5D^o_{4,3,2,1,0}$ [21]. Therefore, the singlet states which occur below the second ionization limit are forbidden to autoionize in LS coupling. Deviations from LS coupling allow autoionization into a continuum with different values of L and S. However, the parity- and J-selection rules must still be conserved. The total angular momentum quantum numbers of the Rydberg states which occur below the second ionization limit ($^2D^o$) are listed in Ref. [9]. It is found that there are accessible continua for each Rydberg state, which allow autoionization beyond LS coupling. Therefore, autoionization can play a role in the $nd'\,^1P^o_1$ series, since all members of this series occur exclusively in absorption and the $3d'$ line is diffuse [9]. This result has been confirmed by emission measurements, where lines involving the $3d'\,^1P^o_1$ state did not occur [8]. It has been suggested that the $nd'\,^1P^o_1$ state may adopt some of the properties of the close-lying $nd'\,^3D^o_1$ state, so that this channel becomes accessible for autoionization. Term interactions have also been considered to account for LS-forbidden autoionization of O(^3P) [37].

In the case of O(^1D), additional optically allowed $^1F^o_3$, $^1D^o_2$, $^1P^o_1$, and $^1S^o_0$ continua exist above the $^2D^o$-ionization limit. All singlet Rydberg states that are observed in optical spectroscopy above the $^2D^o$ limit belong to one of these terms so that autoionization is fully allowed within the LS-coupling scheme.

Absolute photoionization cross sections of O(^1D) have been calculated above the $^2D^o$-ionization limit, which also includes the autoionizing resonances [16,17]. These data include the absolute photoionization cross section near 15.13 eV, where the $(^2P^o)3d''\,^1D^o_2$ Rydberg state occurs (see Fig. 2) [9]. For further analysis of the present results, it is assumed that the optical-absorption oscillator strength f_{abs} entirely contributes to autoionization. This appears to be plausible for allowed autoionization processes, since radiationless transition rates are typically at least three orders of magnitude larger than the radiative rates [38]. We estimate the oscillator strength associated with the $(^2P^o)3d''\,^1D^o_2$ Rydberg transition to be of the order of ≈ 0.015. This follows from the integrated area of this transition above the underlying $^2D^o$ continuum [16,17,39,40]. We note that this is only a rough estimate, since interactions between the $3d''$ $^1D^o_2$ state and the underlying $^2D^o$ continuum are not considered. However, this estimate provides a means to calibrate the fraction of the oscillator strength that contributes to autoionization (f_{auto}) of Rydberg states *below* the $^2D^o$-ionization limit, where radiative decay processes may compete with autoionization. The vertical axis of Fig. 2 has been scaled so that the area under the $3d''$ signal at 15.13 eV is equal to the corresponding integrated photoionization cross section according to Refs. [16,17,40]. It turns out that different autoionization efficiencies of the Rydberg states under investigation are found by comparing the relative areas of the experimental autoionization resonances with the optical oscillator strengths (f_{abs}), which have been compiled recently [18]. Low wavelength resolution of the present results requires us to consider in some cases the sum of oscillator strengths of close-lying lines that are blended in the experimental spectrum. The results are shown in Table I. It is found for the $(^2D)3d'$ and the $(^2D)4d'$ transition that $f_{\mathrm{auto}} \approx f_{\mathrm{abs}}$. Thus, autoionization is the dominant decay route of these transitions. However, f_{auto} is significantly decreased for the ns' and ns'' series, so that competing radiative decay processes are expected to play a more significant role. For example, we estimate for the $3s''$ Rydberg state that $\approx 50\%$ of the calculated optical oscillator strength is due to autoionization. In contrast, emission apparently dominates the $4s'$ state, since it is quite weak in autoionization (cf. Fig. 2). Consistently, this transition is found in emission with high intensity [9].

TABLE I. Comparison of experimental oscillator strengths, which are assigned to autoionization (f_{auto}), with calculated optical oscillator strengths (f_{abs}) obtained from [18].

State	Energy (eV)	f_{auto}	f_{abs}
$3s''$	12.40	0.021	0.046
$4s'$	13.26	0.004	0.017
$3d'$	13.45	0.037	0.038
$4d'+5s'$	14.12	0.025	0.026
$5d'+6s'$	14.43	0.011	0.014
$3d''$	15.13	0.015	0.015

Direct photoionization of O(^1D) into the $^2D^o$ continuum is expected to occur at 14.975 eV [9]. The onset of the ionization continuum is clearly observed in Fig. 2 near ≈ 15 eV. We note that the threshold of direct photoionization cannot be determined from Fig. 2 from the convergence limit of the $n\ell'$ Rydberg series. This is mostly due to the fact that the average oscillator strength of the Rydberg transitions ($\Delta f/\Delta E$) converges smoothly to df/dE at the ionization threshold.

The absolute calibration of the relative intensity scale of the spectrum shown in Fig. 2 can be performed by using the calculated oscillator strength of the $3d''$ Rydberg state at $E = 15.13$ eV. This leads to a photoionization cross section of ≈ 9 Mb in the $^2D^o$ continuum. This value appears to be in reasonable agreement with previous calculations [16,17]. However, we note that no further increase of the ionization continuum intensity is found above the $^2P^o$ threshold that occurs at $E = 16.668$ eV [9]. This is unlike previous results that come from theoretical work, where an increase of the ionization cross section from 7 Mb to ≈ 10 Mb was predicted [16,17,40]. We assume that we cannot find this feature as a result of limited XUV-photon flux at short wavelengths of the present experimental setup.

IV. CONCLUSION

Single-photon induced ionization of O(^1D) has been investigated in the energy regime 12–18 eV. Direct photoion-

ization is not observed between the first ($^4S^o$) and the second ($^2D^o$) ionization continuum, which is in agreement with spin-selection rules. Autoionization of Rydberg states is observed below the $^2D^o$-ionization limit. This process is rationalized in terms of autoionization selection rules, which go beyond simple LS coupling. The relative intensities of the experimental autoionization resonances are compared to optical oscillator strengths that were obtained from theoretical work. Significant differences between the experimental and theoretical results are rationalized in terms of different autoionization efficiencies of the resonantly excited Rydberg singlet states by the $^4S^o$ continuum, which competes with radiative relaxation.

ACKNOWLEDGMENTS

We thank J. Berkowitz for valuable comments and suggestions. Financial support by the Bundesministerium für Bildung und Forschung (bmb+f) (Ozonforschungsprogramm, Grant No. 01 LO 9610/3) and the Fonds der Chemischen Industrie is gratefully acknowledged.

[1] S. T. Amimoto, A. P. Force, R. G. Gulotty, Jr., and J. R. Wiesenfeld, J. Chem. Phys. **71**, 3640 (1979); R. Atkinson, D. L. Baulch, R. A. Cox, R. F. Hampson, Jr., J. A. Kerr, and J. Troe, J. Phys. Chem. Ref. Data **21**, 1125 (1992), and references therein.

[2] G. Brasseur and S. Solomon, *Aeronomy of the Middle Atmosphere* (Reidel, Dordrecht, 1986).

[3] P. G. Burke, W. B. Eissner, D. G. Hummer, and I. C. Percival, *Atoms in Astrophysics* (Plenum, New York, 1983).

[4] H. G. Kuhn, *Atomic Spectra* (Longmans, London, 1962).

[5] E. U. Condon and H. Odabasi, *Atomic Structure* (Cambridge University Press, Cambridge, 1980).

[6] S. Bashkin and J. O. Stoner, *Atomic Energy-Levels and Grotrian Diagrams* (North-Holland, Amsterdam, 1975).

[7] K. B. S. Erikson, Ark. Fys. **30**, 199 (1965).

[8] K. B. S. Eriksson and H. B. S. Isberg, Ark. Fys. **37**, 221 (1968).

[9] R. E. Huffman, J. C. Larrabee, and Y. Tanaka, J. Chem. Phys. **47**, 4462 (1967).

[10] S. T. Pratt, P. M. Dehmer, and J. L. Dehmer, Phys. Rev. A **43**, 282 (1991).

[11] S. T. Pratt, P. M. Dehmer, and J. L. Dehmer, Phys. Rev. A **43**, 4702 (1991).

[12] R. C. Richter and A. J. Hynes, J. Phys. Chem. **100**, 8061 (1996).

[13] R. J. W. Henry, Planet. Space Sci. **15**, 1747 (1967).

[14] G. M. Thomas and T. M. Helliwell, J. Quant. Spectrosc. Radiat. Transf. **10**, 423 (1970).

[15] J. U. Koppel, J. Chem. Phys. **55**, 123 (1971).

[16] K. L. Bell, P. G. Burke, A. Hibbert, and A. E. Kingston, J. Phys. B **22**, 3197 (1989).

[17] K. Butler and C. J. Zeippen, Astron. Astrophys. **234**, 569 (1990).

[18] W. L. Wiese, J. R. Fuhr, and T. M. Deters, J. Phys. Chem. Ref. Data Monogr. **7**, 1 (1996).

[19] F. J. Comes, F. Speier, and A. Elzer, Z. Naturforsch. A **23a**, 125 (1968).

[20] R. E. Huffman, J. C. Larrabee, and Y. Tanaka, J. Chem. Phys. **46**, 2213 (1967).

[21] P. M. Dehmer, J. Berkowitz, and W. A. Chupka, J. Chem. Phys. **59**, 5777 (1973).

[22] P. M. Dehmer and W. A. Chupka, J. Chem. Phys. **62**, 584 (1975).

[23] P. M. Dehmer, W. L. Luken, and W. A. Chupka, J. Chem. Phys. **67**, 195 (1977).

[24] P. K. Carroll and E. T. Kennedy, Contemp. Phys. **22**, 61 (1981).

[25] C. Heckenkamp, U. Heinzmann, G. Schönhense, D. D. Burgess, A. P. Thorne, and J. E. G. Wheaton, J. Phys. D **14**, L203 (1981).

[26] E. T. Kennedy, Contemp. Phys. **25**, 31 (1984).

[27] J. T. Costello, J.-P. Mosnier, E. T. Kennedy, P. K. Carroll, and G. O'Sullivan, Phys. Scr. **T34**, 77 (1991).

[28] R. Flesch, M. C. Schürmann, M. Hunnekuhl, H. Meiss, J. Plenge, and E. Rühl, Rev. Sci. Instrum. **71**, 1319 (2000).

[29] R. Flesch, B. Wassermann, B. Rothmund, and E. Rühl, J. Phys. Chem. **98**, 6263 (1994).

[30] R. Flesch, M. C. Schürmann, J. Plenge, M. Hunnekuhl, H. Meiss, M. Bischof, and E. Rühl, Phys. Chem. Chem. Phys. **1**, 5423 (1999).

[31] J. A. R. Samson, *Techniques of Vacuum Ultraviolet Spectroscopy* (Wiley, New York, 1967).

[32] M. J. Weiss, J. Berkowitz, and E. H. Appelman, J. Chem. Phys. **66**, 2049 (1977).

[33] J. I. Steinfeld, S. M. Adler-Golden, and J. W. Gallagher, J. Phys. Chem. Ref. Data **16**, 911 (1987); B. W. DeMore, S. P. Sander, C. J. Howard, A. R. Ravishankara, D. M. Golden, C. E. Kolb, R. F. Hampson, M. J. Kurylo, and M. J. Molina, *Chemical Kinetics and Photochemical Data for Use in Stratospheric Modeling*, Evaluation No. 12, JPL Publication No. 97-4 (Jet Propulsion Laboratory, Pasadena, 1997).

[34] H. Park and T. G. Slanger, J. Chem. Phys. **100**, 287 (1994); R. L. Miller, A. G. Suits, P. L. Houston, R. Toumi, J. A. Mack, and A. M. Wodtke, Science **265**, 1831 (1994).

[35] K. P. Huber and G. Herzberg, *Molecular Spectra and Molecular Structure, IV. Constants of Diatomic Molecules* (Van Nostrand, New York, 1979).

[36] D. R. Lide, *CRC Handbook of Chemistry and Physics* (CRC Press, Boca Raton, FL, 1992).

[37] A. K. Pradhan and H. E. Saraph, J. Phys. B **10**, 3365 (1977).

[38] J. Berkowitz, J. Phys. B **30**, 583 (1997).

[39] W. Cunto and C. Mendoza, Rev. Mex. Astron. Astrofis. **23**, 107 (1992).

[40] http://cd.sweb.u-strasbg.fr/topbase.html.